THE JOURNAL OF PHYSICAL CHEMISTRY A
A JOURNAL OF THE AMERICAN CHEMICAL SOCIETY

pubs.acs.org/JPCA

Article

Graph-|Q⟩⟨C|: A Quantum Algorithm with Reduced Quantum Circuit Depth for Electronic Structure

Published as part of The Journal of Physical Chemistry virtual special issue "Physical Chemistry of Quantum Information Science".

Srinivasan S. Iyengar,* Juncheng Harry Zhang, Debadrita Saha, and Timothy C. Ricard

Cite This: *J. Phys. Chem. A* 2023, 127, 9334–9345

Read Online

ACCESS | Metrics & More | Article Recommendations | Supporting Information

ABSTRACT: The accurate determination of chemical properties is known to have a critical impact on multiple fundamental chemical problems but is deeply hindered by the steep algebraic scaling of electron correlation calculations and the exponential scaling of quantum nuclear dynamics. With the advent of new quantum computing hardware and associated developments in creating new paradigms for quantum software, this avenue has been recognized as perhaps one way to address exponentially complex challenges in quantum chemistry and molecular dynamics. In this paper, we discuss a new approach to drastically reduce the quantum circuit depth (by several orders of magnitude) and help improve the accuracy in the quantum computation of electron correlation energies for large molecular systems. The method is derived from a graph-theoretic approach to molecular fragmentation and enables us to create a family of projection operators that decompose quantum circuits into separate unitary processes. Some of these processes can be treated on quantum hardware and others on classical hardware in a completely asynchronous and parallel fashion. Numerical benchmarks are provided through the computation of unitary coupled-cluster singles and doubles (UCCSD) energies for medium-sized protonated and neutral water clusters using the new quantum algorithms presented here.

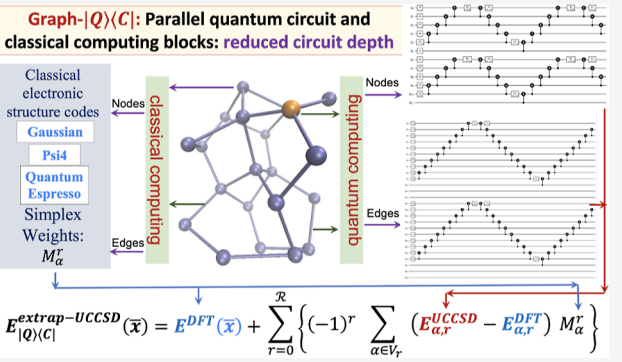

1. INTRODUCTION

Accurate and efficient computation of electron correlation and nuclear dynamics is central to modern computational quantum chemistry, with ongoing impact on materials,[1−3] biological,[4−10] and atmospheric[11−13] processes. However, such studies are limited by (a) the steep algebraic scaling of electron correlation methods[14−18] and (b) the exponential scaling of quantum nuclear dynamics.[19−25] Several classical algorithms have been developed that reduce the scaling for electronic structure and nuclear dynamics.[20,26−34]

Orthogonally, the promise of solving exponentially hard problems using novel quantum hardware and quantum software is a rapidly evolving frontier.[35,36] Many quantum computing technologies, such as ion-traps,[37−40] superconducting coils,[41,42] Bosonic processors with photons,[43−45] solid-state devices and quantum dots inside cavities,[46−49] and Rydberg atoms[50−52] have emerged as potential computational platforms. In addition, algorithms to approximate electron correlation[53−80] for small molecules and quantum nuclear dynamics problems[81−89] have been implemented on quantum hardware devices.

However, critical challenges remain. Here, we discuss one such challenge, namely, the rapid increase in quantum circuit depth in quantum chemistry problems and associated methods that help alleviate this challenge. Consequently, this article is organized as follows: In Section 2 we explain the critical underpinnings behind the increase in quantum circuit depth in electronic structure calculations. Given these challenges, in Section 3 we outline a hybrid quantum/classical algorithm based on a graph-theoretic decomposition of molecular structure to perform electron correlation calculations on an ensemble of quantum and classical hardware systems. The algorithm is also explained in detail in refs 79 and 80 and called "graph-|Q⟩⟨C|" and contains independent sets of classical and quantum algorithmic components within one umbrella.[79,80] In Section 3.1, we also show how graph-|Q⟩⟨C| can be used to provide a quantum algorithm for many-body expansions. In Section 4, we present our results from our quantum algorithm for medium-

Received: June 25, 2023
Revised: October 2, 2023
Published: October 31, 2023

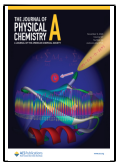

https://doi.org/10.1021/acs.jpca.3c04261
J. Phys. Chem. A 2023, 127, 9334−9345

sized protonated and neutral water clusters. We show that graph-$|Q\rangle\langle C|$ reduces the quantum circuit depth problem, shown in Table 1, by several orders of magnitude while providing millihartree accuracy. Conclusions are given in Section 5.

Table 1. Quantum Circuit Depth Complexity, Represented through the Number of CNOT Gates Needed for Minimal Basis Electronic Structure Calculations for H_2-Clusters and Water Clusters[a]

system	#CNOT gates
H_2	3
$[H_2]_2$	615
$[H_2]_3$	4684
$[H_2]_4$	16,285
$[H_2]_5$	47,312
$[H_2]_6$	107,190
$[H_2]_7$	205,192
$[H_2]_8$	389,472
H_2O	5678
$(H_2O)H^+$	14,842
$(H_2O)_2$	137,468
$(H_2O)_2H^+$	722,044

[a]Quantum circuit depth grows prohibitively with the system size.

2. RAPID GROWTH OF CIRCUIT DEPTH IN QUANTUM COMPUTATION

Most efforts at computing electronic structure on quantum hardware are hindered by the depth of quantum circuits.[21,35,36,79,80,90] Consequently, the complexity of the circuit, combined with limited gate fidelities on quantum hardware, leads to an enormous increase in error.

In Table 1, we show how the standard quantum circuit models[91] available to study electronic structure leads to a rapid increase in the quantum circuit depth and the number of CNOT gates, which greatly affects accuracy. The data in Table 1 is obtained as follows. (a) Hartree−Fock orbitals for each system are precomputed on classical hardware. (b) The second-quantized Fermionic Hamiltonian consistent with a unitary coupled cluster (UCC) wave function ansatz[92,93] is then converted into quantum circuits using the software development kit, Qiskit,[91] using a parity mapping protocol.[94] (c) The quantum circuits are then executed on a Qiskit built-in state-vector simulator. The resultant energies are optimized using the sequential least-squares programming (SLSQP) optimizer.[68,95] No noise model is used in these simulations. The corresponding circuit parameters are listed in Table 1.

This rapid increase in circuit depth is also consistent with the theory behind quantum Shannon decomposition,[96,97] which allows one to decompose an arbitrary unitary system into a set of universal gates using an alternating sequence of cosine−sine decomposition[98] and multiplexor demultiplexing methods.[97] Briefly, though, a system with N qubits needs a 2^N by 2^N evolution operator which has in general $\approx 4^N$ elements that describe the time-evolution of the system. Hence, an arbitrary problem can have an exponential number of parameters necessitating an exponential number of gates, and this may also be indicated by the data from Qiskit in Table 1. Additionally, Table 1 is also consistent with ref 99, where the authors show the exponential scaling in the number of two-qubit gates for UCCSD-VQE.

The rapid increase in the CNOT gate count shown in Table 1 contributes to an accumulation of error in the following ways. Quantum gate fidelity for CNOT gates is roughly 95%[64,100] since these require maximally entangling $XX(\pi/2)$ gates that have lower quality performance[64] compared to small angle XX gates. The associated increase in error, as shown in Table 1, restricts both the size and the quality of performance. Thus, despite the growing number of available quantum hardware platforms and accompanying quantum algorithms, performing accurate quantum chemical calculations remains a significant challenge.

3. GRAPH-$|Q\rangle\langle C|$ ALGORITHM

This section is organized as follows: In Section 3.1 we discuss a general projection operator formalism that helps decompose any complex quantum circuit into a family of circuits of much lower complexity. This approach is used to provide efficient algorithms for many-body theory (Section 3.2, also see Section S.I. in the Supporting Information) and ONIOM[101]-type extrapolation of correlation energy (Section 3.3). Computational details are discussed in Section S.I. In essence, as part of Section 3.3 the overall computational workload is partitioned into (a) classical computing sections to be carried out on traditional classical electronic structure platforms, such as Gaussian,[102] Psi4,[103] Orca,[104] and Quantum Espresso,[105] and (b) quantum computing sections to be carried out using quantum circuit models. Graph-$|Q\rangle\langle C|$ is quantum hardware agnostic and is designed to be used on an ensemble of quantum hardware simultaneously and asynchronously for a given calculation.

3.1. Projected Reduced-Depth Quantum Circuits from Hilbert Space Decomposition Using Venn Diagrams and Graphs. We begin with a Venn diagram that divides a coordinate representation $|x\rangle\langle x|$ into regions, A, B, C, etc. In Figure 1a, we superimposed the Venn diagram on a protonated water cluster. The Venn diagram divides a molecular system into several regions. Using the principle of inclusion−exclusion,[106] the resolution of the identity for the Hilbert space depicted within the Venn diagram may be written as

$$\begin{aligned}\mathbf{I} &\equiv \int_{A\cup B\cup C} dx|x\rangle\langle x| \\ &= \int_A dx|x\rangle\langle x| + \int_B dx|x\rangle\langle x| + \int_C dx|x\rangle\langle x| - \\ &\int_{A\cap B} dx|x\rangle\langle x| - \int_{A\cap C} dx|x\rangle\langle x| - \int_{B\cap C} dx|x\rangle\langle x| + \\ &\int_{A\cap B\cap C} dx|x\rangle\langle x| \\ &= \mathcal{P}_A + \mathcal{P}_B + \mathcal{P}_C - \mathcal{P}_{A\cap B} - \mathcal{P}_{A\cap C} - \mathcal{P}_{B\cap C} \\ &\quad + \mathcal{P}_{A\cap B\cap C} \end{aligned} \tag{1}$$

where we have introduced projection operators

$$\mathcal{P}_A \equiv \int_A dx|x\rangle\langle x| \tag{2}$$

that project portions of the Hilbert space. The left side of eq 1 is the identity, and it sums over the entire space represented here by the set $A \cup B \cup C$.

https://doi.org/10.1021/acs.jpca.3c04261
J. Phys. Chem. A 2023, 127, 9334−9345

While eq 1 arises from the inclusion−exclusion principle[106] and can be generalized to an arbitrary number of sets, an alternate approach to divide the molecular space can be obtained by introducing a graph decomposition of molecular structure. Toward this, a molecular assembly is partitioned into a set of regions to be represented as nodes, or vertices in a graph. These nodes may be defined based on chemistry or by using a numerical criterion. First-order interactions between these discrete nodes may be captured by creating edges that are the union of nodes. The set of nodes and edges are represented as $\mathbf{V_0}$ and $\mathbf{V_1}$, respectively, and together define a graph, $\mathcal{G} \equiv \{\mathbf{V_0}; \mathbf{V_1}\}$, illustrated on the left side in Figure 2 and in Figure 1c. However, such a graph also contains a set of higher-order rank-r objects, $\mathbf{V}_r$, known as simplexes[107−109]

$$\{\mathbf{V}_r | r = 0,1,2, \ldots\} \equiv \{\mathbf{V_0}, \mathbf{V_1}, \mathbf{V_2}, \ldots\} \tag{3}$$

and these capture higher-order interactions between nodes. Simplexes are geometric objects with an arbitrary number of vertices, where all pairs of vertices are connected.[107−109]

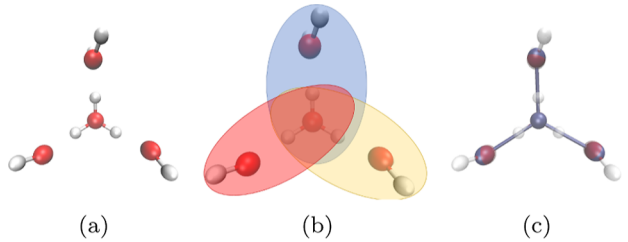

Figure 1. Sets *A*, *B*, and *C* are illustrated for a protonated water cluster, with graphical representation in (c).

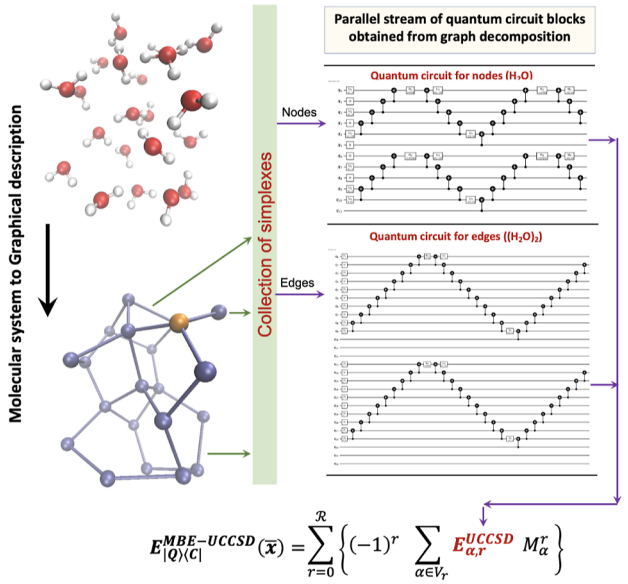

Figure 2. Implementing eqs 5 and 7 on quantum hardware using the graph partitioning approach. Using the projection operators in eq 5, the overall molecular unitary operator, $\mathcal{U}$, may be represented using a family of independent unitary operators $\{\mathcal{U}_{\alpha,r}\}$, that may be processed in parallel as shown. The associated family of independent quantum circuits is shown on the right side, one circuit for each fragment.

Using the graph-theoretic decomposition, an equivalent expression for the resolution of the identity, as in eq 1, may be obtained using projectors that encompass nodes, edges, and higher-order simplexes as

$$\begin{aligned} \mathbf{I} &= \sum_{\alpha \in \mathbf{V_0}} \mathcal{M}^0_\alpha \mathcal{P}_{\alpha,0} - \sum_{\alpha \in \mathbf{V_1}} \mathcal{M}^1_\alpha \mathcal{P}_{\alpha,1} + \\ &\quad \sum_{\alpha \in \mathbf{V_2}} \mathcal{M}^2_\alpha \mathcal{P}_{\alpha,2} - \cdots \\ &= \sum_{r=0}^{\mathcal{R}} (-1)^r \sum_{\alpha \in \mathbf{V_r}} \mathcal{M}^r_\alpha \mathcal{P}_{\alpha,r} \end{aligned} \tag{4}$$

where, $\mathcal{M}^r_\alpha$ is the number of times the α^{th} rank-r term (in $\mathbf{V_r}$) appears in all rank-m terms (in $\mathbf{V_m}$), for $m \geq r$.

We now introduce a quantum circuit depicted by $\mathcal{U}$, a unitary operator, that propagates the electronic structure for the full molecular system. As noted above, the complexity of such a circuit and the associated resources may grow rapidly as the system size grows. To overcome this, we apply the graph-theoretically defined resolution of identity in eq 4 to $\mathcal{U}$

$$\begin{aligned} \mathbf{I}\mathcal{U} &= \sum_{r=0}^{\mathcal{R}} (-1)^r \sum_{\alpha \in \mathbf{V_r}} \mathcal{M}^r_\alpha [\mathcal{P}_{\alpha,r} \mathcal{U}] \\ &= \sum_{r=0}^{\mathcal{R}} (-1)^r \sum_{\alpha \in \mathbf{V_r}} \mathcal{M}^r_\alpha \mathcal{U}_{\alpha,r} \end{aligned} \tag{5}$$

where

$$\mathcal{U}_{\alpha,r} \equiv \mathcal{P}_{\alpha,r} \mathcal{U} \tag{6}$$

and these represent a family of projected quantum circuits, one for each molecular fragment, as illustrated in Figure 2.

3.2. Quantum Circuits for Many-Body Theory. We use the individual quantum circuits, $\{\mathcal{U}_{\alpha,r}\}$, to obtain a family of fragment energies. In this publication, a UCCSD wave function ansatz is used to construct the quantum algorithm, but this is not a requirement. (Computational aspects are discussed in Supporting Information, Section S.II.). As a result, the energies obtained from the $\{\mathcal{U}_{\alpha,r}\}$ quantum calculations are referred to as $\{E^{\text{UCCSD}}_{\alpha,r}\}$. When these energies are used in eq 5, we obtain

$$E^{\text{MBE-UCCSD}}_{|Q\rangle\langle C|} = \sum_{r=0}^{\mathcal{R}} (-1)^r \sum_{\alpha \in \mathbf{V_r}} E^{\text{UCCSD}}_{\alpha,r} \mathcal{M}^r_\alpha \tag{7}$$

Equation 7 yields a parallel stream of multiple quantum processes as illustrated in Figures 2 and 3. It is critical to note that these independent circuits, $\{\mathcal{U}_{\alpha,r}\}$, are for much smaller fragments as compared to the full system of interest. Hence, one may expect, based on Table 1, the error in propagation to be limited. Indeed, we find this to be the case in Section 4. However, eq 7 is also closely related to the standard many-body expansions.[110−114] The details of this connection are presented in Supporting Information S.II.

A critical underpinning of our graph-theoretic formalism arises from the fact that simplexes are closed convex hulls.[107,108] For instance, a rank-r object containing some collection of r nodes is considered to be a simplex only if all pairs of nodes within it are connected through edges.

This requirement is the single main constraint and is a critical feature of our algorithm.

3.3. Improving Quantum-MBE through Extrapolation. In refs 115 and 116, it has been shown that the accuracy of eq 7 can be improved[115−126] through a composite expression[127−131] that contains a perturbative ONIOM-type[101] correction to a

https://doi.org/10.1021/acs.jpca.3c04261
J. Phys. Chem. A 2023, 127, 9334−9345

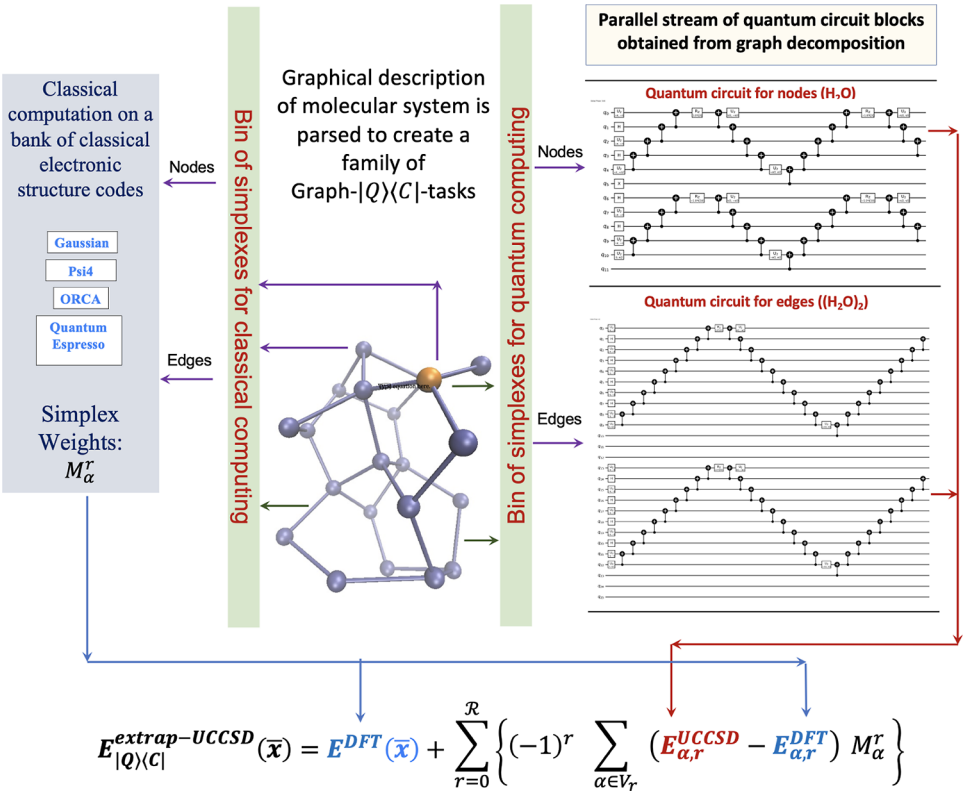

Figure 3. Illustration of Graph-$|Q\rangle\langle C|$ for eqs 10 and 11. The quantum circuit decomposition on right (also see Figure 2) helps compute $\{E^{\mathrm{UCCSD}}_{\alpha,r};E^{\mathrm{UCCSD}}_{\alpha,r,|Q\rangle}\}$ in eqs 10 and 11. Classical algorithms (left) help compute $\{E^{\mathrm{DFT}}_{\alpha,r};E^{\mathrm{DFT}}\}$ (in eq 10 and $\{E^{\mathrm{DFT}}_{\alpha,r};E^{\mathrm{DFT}}_{\alpha,r,|C\rangle};E^{\mathrm{UCCSD}}_{\alpha,r,|C\rangle};E^{\mathrm{DFT}}_{\alpha,r,|C\rangle}\}$ (in eq 11).

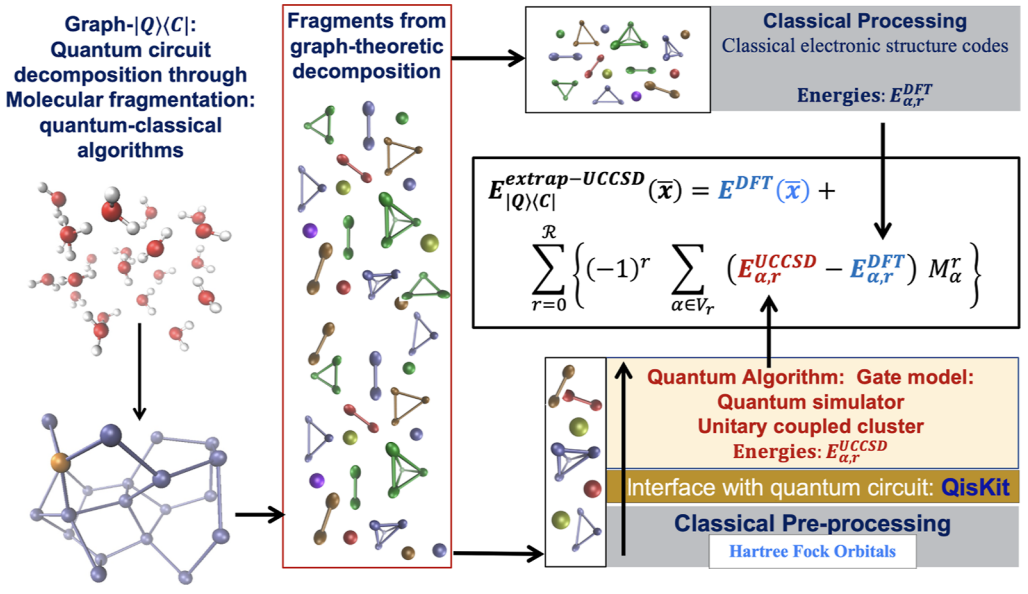

Figure 4. Algorithmic flow for graph-$|Q\rangle\langle C|$: the classical and quantum processes are asynchronous.

lower level approximation. The perturbative correction is the difference between two many body expansions

$$E^{\mathrm{extrap-UCCSD}}_{|Q\rangle\langle Cl}(\bar{\mathbf{x}}) = E^{\mathrm{DFT}}(\bar{\mathbf{x}}) + E^{\mathrm{MBE-UCCSD}}_{|Q\rangle\langle Cl}(\bar{\mathbf{x}}) - E^{\mathrm{DFT}}_{\mathrm{MBE}}(\bar{\mathbf{x}}) \quad (8)$$

where the left side, $E^{\mathrm{extrap-UCCSD}}_{|Q\rangle\langle Cl}(\bar{\mathbf{x}})$, is the graph-theoretically obtained many-body extrapolation to UCCSD, and the term $E^{\mathrm{MBE-UCCSD}}_{|Q\rangle\langle Cl}(\bar{\mathbf{x}})$ on the right side incorporates the value from eq 7 at geometry $\bar{\mathbf{x}}$. The quantity, $E^{\mathrm{DFT}}_{\mathrm{MBE}}(\bar{\mathbf{x}})$ is computed classically according to

$$E^{\mathrm{DFT}}_{\mathrm{MBE}} = \sum_{r=0}^{\mathcal{R}} (-1)^r \sum_{\alpha\in \mathbf{V}_r} E^{\mathrm{DFT}}_{\alpha,r} \mathcal{M}^r_\alpha \quad (9)$$

The resultant algorithm is shown in Figure 4 and involves the asynchronous processing of several classical and quantum computations of lower complexity. The resultant final energy

https://doi.org/10.1021/acs.jpca.3c04261
J. Phys. Chem. A 2023, 127, 9334−9345

expression in eq 8, or the one obtained from combining eqs 7−9, that is

$$E^{\text{extrap}-\text{UCCSD}}_{|Q\rangle\langle C|}(\bar{\mathbf{x}}) = E^{\text{DFT}}(\bar{\mathbf{x}}) + \sum_{r=0}^{\mathcal{R}} (-1)^r \sum_{\alpha\in\mathbf{V}_r} (E^{\text{UCCSD}}_{\alpha,r} - E^{\text{DFT}}_{\alpha,r})\mathcal{M}^r_\alpha \tag{10}$$

is closely related to other ONIOM-based[101,131−137] molecular fragmentation methods[113,114,131,137−149] and developments in many-body theory.[110−114,150−156] The closely related quantum embedding methods[157−163] have been used for quantum computing applications.[162,163] However, most embedding methods[162] generally allow the description of a chosen part of a system accurately while retaining the description of the environment at a lower level. Indeed, such methods are extremely powerful. The method discussed here, however, is based on the need to describe a full, and potentially large, system at a high level of theory but at lower computational complexity. The approach has been described in detail for classical computing in refs 115−124, and here we utilize this approach to reduce the complexity of quantum circuit-based computing.

Additionally, given the current challenges in quantum computing, in this publication, we perform all $\{E^{\text{UCCSD}}_{\alpha,r}\}$ calculations as outlined in Figures 2 and 3, up to a maximum rank of $r = \mathcal{R}_{|Q\rangle}$ using quantum circuits. Thus, the form of eq 10 that is implemented here is

$$E^{\text{extrap}-\text{UCCSD}}_{|Q\rangle\langle C|}(\bar{\mathbf{x}}) = E^{\text{DFT}}(\bar{\mathbf{x}}) + \sum_{r=0}^{\mathcal{R}_{|Q\rangle}} (-1)^r \sum_{\alpha\in\mathbf{V}_r} (E^{\text{UCCSD}}_{\alpha,r,|Q\rangle} - E^{\text{DFT}}_{\alpha,r,|C\rangle})\mathcal{M}^r_\alpha + \sum_{r=\mathcal{R}_{|Q\rangle}+1}^{\mathcal{R}} (-1)^r \sum_{\alpha\in\mathbf{V}_r} (E^{\text{UCCSD}}_{\alpha,r,|C\rangle} - E^{\text{DFT}}_{\alpha,r,|C\rangle})\mathcal{M}^r_\alpha \tag{11}$$

where $|Q\rangle$ or $|C\rangle$ is used to denote quantum or classical processing. Thus, for $r \le \mathcal{R}_{|Q\rangle}$, $\{E^{\text{UCCSD}}_{\alpha,r}\}$ are obtained using quantum algorithms, whereas for $r > \mathcal{R}_{|Q\rangle}$, $\{E^{\text{UCCSD}}_{\alpha,r}\}$ are obtained using classical algorithms.

4. STUDIES ON WATER CLUSTERS USING QUANTUM ALGORITHMS

We have applied graph-$|Q\rangle\langle C|$ to a range of protonated and neutral water cluster problems.[164−170] Water clusters are found in biological membranes and enzyme active sites,[164,165] photosynthetic reaction center of Rhodobacter sphaeroides,[164] ion channels,[166] and fuel cells.[170] These have also been incorporated into carbon nanotubes.[167−169] The mass of the hydrogen nucleus makes quantum nuclear effects critical;[171−174] additionally, multidimensional quantum nuclear effects are also known to be critical in such systems.[175,176] While the key properties here involve detailed study of electronic and nuclear degrees of freedom,[33,177] with quantum algorithms for such applications discussed in refs 88 and 89, here, we discuss the accuracy and efficiency of graph-$|Q\rangle\langle C|$ in obtaining post-Hartree−Fock (coupled cluster) energies for such polarized systems.

Protonated water clusters of various sizes have been studied here with graph-$|Q\rangle\langle C|$. Specifically, the analysis of errors due to the truncation in rank ($\mathcal{R}$ in eq 5) and the edge length cutoff used in the graph definition, allows us to gauge the fragment circuit complexity needed to produce milli-hartree accuracy.

The complexity of our algorithm is determined by (a) the maximum value of $\mathcal{R}$ within the family of quantum circuits: $\{\mathcal{U}_{\alpha,r}|_{r=0\cdots\mathcal{R}}\}$, and (b) the maximum edge length used to create the graphs. For the range of systems considered here, the distribution of oxygen−oxygen distances is shown in Figure 5.

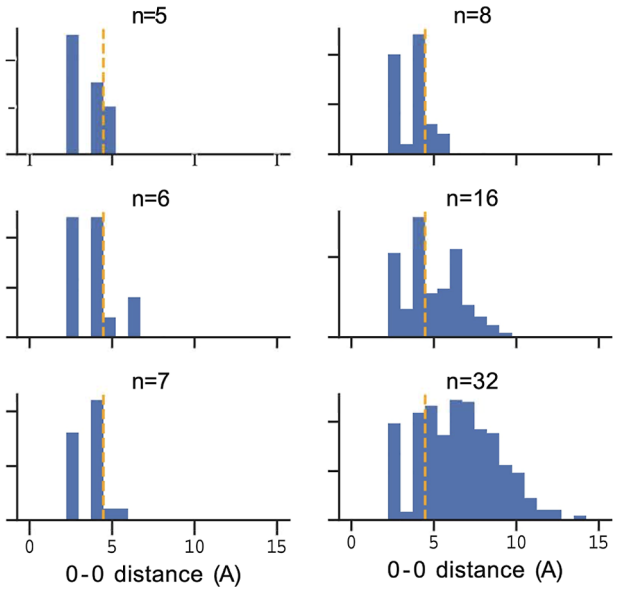

Figure 5. Oxygen−oxygen distribution function for protonated water clusters, $(H_2O)_nH^+$.

The yellow dashed line in these figures shows the edge cutoff length chosen in this study. As this edge cutoff length is increased, it has been shown in ref 116 that the accuracy increases provided the maximum value of $\mathcal{R}$ in eqs 7 and 8 is also increased. However, then, the number of fragments grows, and by extension the number of parallel quantum and classical processes also grows as dictated by the algorithm in Figure 4.

A significant challenge addressed in this work arises from the data presented in Table 1. A more detailed set of parameters that dictate the computational complexity is given in Table 2. Clearly, a full system calculation using a quantum circuit model is not only cost-prohibitive at present but also likely to remain challenging, and efficient algorithms such as those presented here and elsewhere[58,60,71,76−78] may allow larger systems to be treated accurately as quantum hardware capabilities develop further.

The set of results for medium and larger water-clusters are presented in Figures 6 and 7. We present the purely classical results in Figures 6a and 7a, where all subprocesses in Figure 4 are treated on classical hardware, using classical algorithms. This baseline establishes the accuracy of the proposed approach. In Figures 6b and 7b, we then supplement our studies by computing only rank-0 (node: H_2O and H_3O^+) clusters using the Qiskit QASM simulator[91] with all other clusters treated classically. That is, as stated in Figure 2, nodes are processed using quantum algorithms, but all other fragments are processed classically for DFT as well as UCCSD energies. Also see Figure 4. As the capabilities of quantum hardware and simulators improve, the load distribution will be adjusted. Furthermore, the error in quantum processing can then be written as the

https://doi.org/10.1021/acs.jpca.3c04261
J. Phys. Chem. A 2023, 127, 9334−9345

Table 2. Quantum Circuit Resource Requirements When Standard Techniques Are Used: Illustration for a Family of H_2-Clusters and Water-Clusters

	factors that determine cost for a standard quantum calculation				
system	circuit depth	number of qubits	number of CNOT gates	total number of gates	number of parameters
H_2	11	2	3	16	3
$(H_2)_2$	924	6	615	1217	26
$(H_2)_3$	5920	10	4684	7370	117
$(H_2)_4$	21,361	14	16,285	27,021	360
$(H_2)_5$	57,402	18	47,312	70,204	875
$(H_2)_6$	128,469	22	107,190	156,081	1818
$(H_2)_7$	253,846	26	205,192	313,143	3381
$(H_2)_8$	458,233	30	389,472	550,279	5792
H_2O	7512	12	5768	8961	140
$(H_3O)^+$	18,302	14	14,842	22,564	315
$(H_2O)_2$	163,099	26	137,468	196,495	2220
$(H_2O)_2H^+$	859,039	28	722,044	2,881,384	3500

difference between energies in eq 10 obtained from graph-$|Q\rangle\langle C|$ (that is, eq 11) and that obtained from classical processing, that is

$$\Delta E_{|Q\rangle\langle C|}(\bar{\mathbf{x}}) = \sum_{r=0}^{\mathcal{R}_{|Q\rangle}} (-1)^r \sum_{\alpha \in \mathbf{V}_r} (E^{\mathrm{UCCSD}}_{\alpha,r,|Q\rangle} - E^{\mathrm{UCCSD}}_{\alpha,r,|C\rangle}) \mathcal{M}^r_\alpha \tag{12}$$

The graph-$|Q\rangle\langle C|$ error in eq 12 not only depends on the errors, $(E^{\mathrm{UCCSD}}_{\alpha,r,|Q\rangle} - E^{\mathrm{UCCSD}}_{\alpha,r,|C\rangle})$, but also the simplex weights, $\mathcal{M}^r_\alpha$, which change as $\mathcal{R}$ increases. At the end, the behavior in Figures 6 and 7 is due to the combination of the systematic error in $E^{\mathrm{UCCSD}}_{\alpha,r,|Q\rangle}$ and the associated weights $\mathcal{M}^r_\alpha$.

As noted in Table 2, as system size grows, the circuit gets extremely complex, so much so that it is not even possible to compute the circuit for many of the larger water clusters treated in this paper. The graph-$|Q\rangle\langle C|$ approach reduces resource complexity in such cases by reducing the overall circuit needs to a family of rank-0 (H_2, H_2O, or $(H_3O)^+$), rank-1 ($(H_2)_2$, $(H_2O)_2$, or $(H_2O)_2H^+$), rank-2 ($(H_2)_3$, $(H_2O)_3$, or $(H_2O)_3H^+$), and rank-3 ($(H_2)_4$, $(H_2O)_4$, or $(H_2O)_4H^+$) terms. For many of the water clusters treated here (such as $(H_2O)_{32}H^+$ in Figure 7), this amounts to a reduction in circuit complexity of several orders of magnitude. Thus, Figure 7 basically says that to obtain sub-kcal/mol accuracy for $(H_2O)_{32}H^+$, quantum circuit complexity need not exceed that of $(H_2O)_4H^+$. This is a significant result in the current publication.

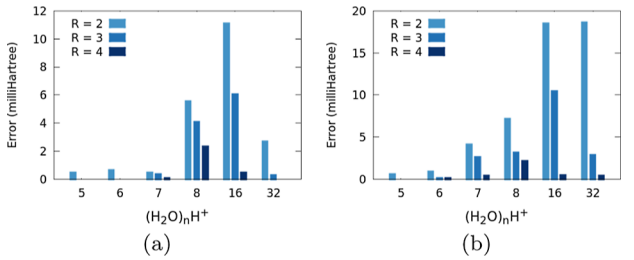

Figure 7. Accuracy of graph-$|Q\rangle\langle C|$ for protonated water clusters, $(H_2O)_nH^+$. The value of "n" is noted along the horizontal axis, and results are presented for three different ranks. (a): classical. (b): graph-$|Q\rangle\langle C|$.

To systematically dissect the contributions from $(E^{\mathrm{UCCSD}}_{\alpha,r,|Q\rangle} - E^{\mathrm{UCCSD}}_{\alpha,r,|C\rangle})$ and $\mathcal{M}^r_\alpha$ toward the total errors captured in Figures 6 and 7, we first note that from the Cauchy inequality,[178] the sum over α term in eq 12 is bounded as per

$$\sum_{\alpha \in \mathbf{V}_r} (E^{\mathrm{UCCSD}}_{\alpha,r,|Q\rangle} - E^{\mathrm{UCCSD}}_{\alpha,r,|C\rangle}) \mathcal{M}^r_\alpha \leq \|(\bar{E}^{\mathrm{UCCSD}}_{r,|Q\rangle} - \bar{E}^{\mathrm{UCCSD}}_{r,|C\rangle})\|_1 \|\mathcal{M}^r_\alpha\|_1 \tag{13}$$

where we have now introduced vectors with index α and interpreted the left side above as a dot product. The quantities of $\|\cdots\|_1$ are the L^1-norm of a vector. Both vectors are of length equal to the number of elements in $\mathbf{V}_0$. It must also be noted that the Cauchy inequality is generally written in terms of the L^2-norm of a vector. However, it is also true that the L^1-norm of a vector is always greater than its L^2-norm, and this is used to obtain eqs 14 and 15. Accordingly, we dissect the contributions to $\Delta E_{|Q\rangle\langle C|}(\bar{\mathbf{x}})$ according to

$$\Delta E_{|Q\rangle\langle C|}(\bar{\mathbf{x}}) \leq \sum_{r=0}^{\mathcal{R}_{|Q\rangle}} (-1)^r \|\bar{E}^{\mathrm{UCCSD}}_{r,|Q\rangle} - \bar{E}^{\mathrm{UCCSD}}_{r,|C\rangle}\|_1 \|\mathcal{M}^r\|_1 \tag{14}$$

or for $\mathcal{R}_{|Q\rangle} = 0$

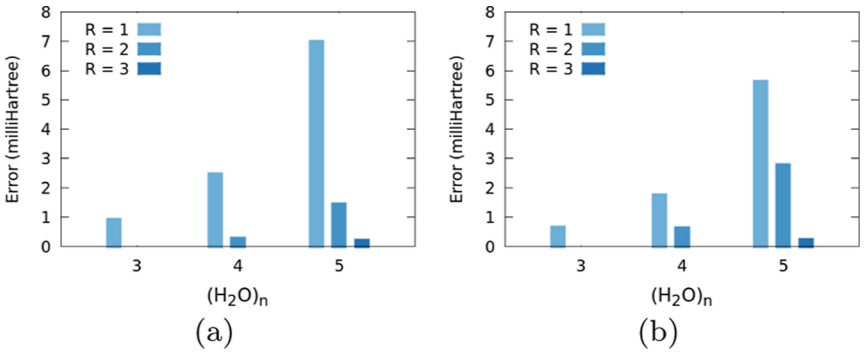

Figure 6. Accuracy of graph-$|Q\rangle\langle C|$ for neutral water clusters, $(H_2O)_n$. The value of "n" is noted along the horizontal axis, and results are presented for two different ranks. (a): classical. (b): graph-$|Q\rangle\langle C|$.

https://doi.org/10.1021/acs.jpca.3c04261
J. Phys. Chem. A 2023, 127, 9334−9345

$$E^{\text{extrap}-\text{UCCSD}}_{|Q\rangle\langle C|}(\bar{\mathbf{x}}) \leq \|(\bar{E}^{\text{UCCSD}}_{r=0,|Q\rangle} - \bar{E}^{\text{UCCSD}}_{r=0,|C\rangle})\|_1 \|\mathcal{M}^{r=0}\|_1 \quad (15)$$

We present the contributions $\|(\bar{E}^{UCCSD}_{r,|Q\rangle} - \bar{E}^{UCCSD}_{r,|C\rangle})\|_1$ and $\|\mathcal{M}^r\|_1$ in Figure 8 to gauge the difference in Figure 7.

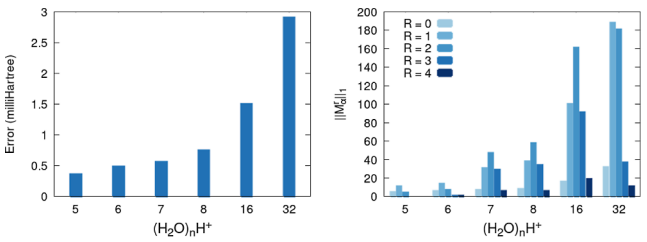

Figure 8. (a) Shows the behavior of $\|(\bar{E}^{UCCSD}_{r=0,|Q\rangle} - \bar{E}^{UCCSD}_{r=0,|C\rangle})\|_1$ in eq 15 as a function of system size for protonated water clusters. (b) Shows the behavior of $\|\mathcal{M}^{r=0}\|_1$. The energy contributions to the error in eq 15 do grow with system size but are controlled to within the milli-hartree scale. However, the multiplicity arising from the graph formalism grows initially with rank and is responsible for the large discrepancy in Figure 7a,b for lower values of $\mathcal{R}$.

Additionally, it is useful to note that the quantity $\|(\bar{E}^{UCCSD}_{r=0,|Q\rangle} - \bar{E}^{UCCSD}_{r=0,|C\rangle})\|_1$ is the error in the $\mathcal{R} = 0$ result. Clearly, the growth in multiplicity is responsible for the large discrepancy in Figure 7a,b for lower values of $\mathcal{R}$.

As the size of the molecular system grows, the corresponding circuit complexity, as represented by the number of CNOT gates, increases exponentially. However, the complexity of graph-$|Q\rangle\langle C|$ only depends on the maximum rank fragment processed on quantum hardware and hence grows in a much more gradual fashion while maintaining accuracy in the milli-hartree range, as can be seen from the figures above. For example, for the protonated water cluster, the theoretical scaling of the current quantum algorithm for the larger water clusters, such as $(H_2O)_{32}H^+$, is due to a protonated tetramer ($(H_2O)_4H^+$) for sub-milli-hartree accuracy. Clearly, these figures also show how our results converge with rank. The resources needed are as dictated by the data in Table 2 and provides a significant reduction in the resources needed to perform these computations.

Thus, in general, choice of maximum $\mathcal{R}$ and the edge length cutoff would be based on a compromise between accuracy and efficiency. However, in all cases, it appears that graph-$|Q\rangle\langle C|$ presents a powerful approach to adaptively tailor the quantum circuit depth.

5. CONCLUSIONS

The potential to address exponentially complex problems using quantum computing is an evolving research frontier,[35] but it is now accepted[35,36] that universal, fully fault-tolerant, quantum computers are a distant dream,[35,36] and new frontiers such as noisy intermediate scale quantum (NISQ)[35] systems have emerged. In this paper, we discuss a novel procedure called graph-$|Q\rangle\langle C|$, which is a hybrid approach to interleave NISQ processors with classical computers as suggested in refs 35 and 36. In doing so, graph-$|Q\rangle\langle C|$ helps greatly reduce the depth of quantum circuits and helps improve the quality of the results in obtaining post-Hartree−Fock electronic structure energies on quantum hardware. This is achieved as follows: A molecular system is divided into overlapping regions through a graph-theoretically generated set of projection operators. These projection operators allow the decomposition of a complex quantum circuit into a parallel stream of processes, some of which can be treated on quantum hardware and others on classical hardware. Thus, graph-$|Q\rangle\langle C|$ can be spawned on to a potentially large ensemble of classical and quantum hardware systems that each carry out tasks in an asynchronous fashion. The approach is demonstrated by computing post-Hartree−Fock electronic energies for a range of water clusters.

■ ASSOCIATED CONTENT

Supporting Information

The Supporting Information is available free of charge at https://pubs.acs.org/doi/10.1021/acs.jpca.3c04261.

Quantum computational aspects associated with the implementation of eqs 10 and 11 and connections between many-body theory and eq 7 (PDF)

■ AUTHOR INFORMATION

Corresponding Author

Srinivasan S. Iyengar − *Department of Chemistry, Department of Physics, and the Indiana University Quantum Science and Engineering Center (IU-QSEC), Indiana University, Bloomington, Indiana 47405, United States;* orcid.org/0000-0001-6526-2907; Email: iyengar@indiana.edu

Authors

Juncheng Harry Zhang − *Department of Chemistry, Department of Physics, and the Indiana University Quantum Science and Engineering Center (IU-QSEC), Indiana University, Bloomington, Indiana 47405, United States*

Debadrita Saha − *Department of Chemistry, Department of Physics, and the Indiana University Quantum Science and Engineering Center (IU-QSEC), Indiana University, Bloomington, Indiana 47405, United States*

Timothy C. Ricard − *Department of Chemistry, Department of Physics, and the Indiana University Quantum Science and Engineering Center (IU-QSEC), Indiana University, Bloomington, Indiana 47405, United States*

Complete contact information is available at: https://pubs.acs.org/10.1021/acs.jpca.3c04261

Notes

The authors declare no competing financial interest.

■ ACKNOWLEDGMENTS

This research was supported by the National Science Foundation grants CHE-2102610 and OMA-1936353 to author S.S.I.

■ REFERENCES

(1) Iannuzzi, M.; Parrinello, M. Proton Transfer in Heterocycle Crystals. *Phys. Rev. Lett.* **2004**, *93*, 025901.

(2) Tse, Y.-L. S.; Herring, A. M.; Kim, K.; Voth, G. A. Molecular Dynamics Simulations of Proton Transport in 3M and Nafion Perfluorosulfonic Acid Membranes. *J. Phys. Chem. C* **2013**, *117*, 8079−8091.

(3) Lin, I.-H.; Lu, Y.-H.; Chen, H.-T. Nitrogen-doped C60 as a robust catalyst for CO oxidation. *J. Comput. Chem.* **2017**, *38*, 2041−2046.

(4) Field, M. J.; Bash, P. A.; Karplus, M. A Combined Quantum Mechanical and Molecular Mechanical Potential for Molecular Dynamics Simulations. *J. Comput. Chem.* **1990**, *11*, 700−733.
(5) Wong, K.-Y.; Gao, J. Insight into the phosphodiesterase mechanism from combined QM/MM free energy simulations. *FEBS J.* **2011**, *278*, 2579−2595.
(6) Harris, D. L. Oxidation and Electronic State Dependence of Proton Transfer in the Enzymatic Cycle of Cytochrome P450eryF. *J. Inorg. Biochem.* **2002**, *91*, 568−585.
(7) Lin, Y.-l.; Gao, J. Kinetic Isotope Effects of L-Dopa Decarboxylase. *J. Am. Chem. Soc.* **2011**, *133*, 4398−4403.
(8) Rega, N.; Iyengar, S. S.; Voth, G. A.; Schlegel, H. B.; Vreven, T.; Frisch, M. J. Hybrid Ab-Initio/Empirical Molecular Dynamics: Combining the ONIOM Scheme with the Atom-Centered Density Matrix Propagation (ADMP) Approach. *J. Phys. Chem. B* **2004**, *108*, 4210−4220.
(9) Iyengar, S. S.; Sumner, I.; Jakowski, J. Hydrogen Tunneling in an Enzyme Active Site: A Quantum Wavepacket Dynamical Perspective. *J. Phys. Chem. B* **2008**, *112*, 7601−7613.
(10) Phatak, P.; Sumner, I.; Iyengar, S. S. Gauging the Flexibility of the Active Site in Soybean Lipoxygenase-1 (SLO-1) Through an Atom-Centered Density Matrix Propagation (ADMP) Treatment That Facilitates the Sampling of Rare Events. *J. Phys. Chem. B* **2012**, *116*, 10145−10164.
(11) Gerber, R. B.; Sebek, J. Dynamics Simulations of Atmospherically Relevant Molecular Reactions. *Int. Rev. Phys. Chem.* **2009**, *28*, 207−222.
(12) Dietrick, S. M.; Pacheco, A. B.; Phatak, P.; Stevens, P. S.; Iyengar, S. S. The Influence of Water on Anharmonicity, Stability and Vibrational Energy Distribution of Hydrogen-Bonded Adducts in Atmospheric Reactions: Case Study of the OH + Isoprene Reaction Intermediate Using *Ab-Initio* Molecular Dynamics. *J. Phys. Chem. A* **2012**, *116*, 399−414.
(13) Hammerich, A. D.; Finlayson-Pitts, B. J.; Gerber, R. B. NO_x Reactions on Aqueous Surfaces with Gaseous HCl: Formation of a Potential Precursor to Atmospheric Cl Atoms. *J. Phys. Chem. Lett.* **2012**, *3*, 3405−3410.
(14) Head-Gordon, M.; Pople, J. A.; Frisch, M. J. MP2 energy evaluation by direct methods. *Chem. Phys. Lett.* **1988**, *153*, 503−506.
(15) Schlegel, H. B.; Frisch, M. J. Computational bottlenecks in molecular orbital calculations. *Theoretical and Computational Models for Organic Chemistry*; Springer, 1991; pp 5−33.
(16) Pople, J. A.; Schlegel, H. B.; Krishnan, R.; DeFrees, D. J.; Binkley, J. S.; Frisch, M. J.; Whiteside, R. A.; Hout, R. F.; Hehre, W. J. Molecular orbital studies of vibrational frequencies. *Int. J. Quantum Chem., Quantum Chem. Symp.* **1981**, *20*, 269−278.
(17) Pople, J. A.; Krishnan, R.; Schlegel, H. B.; Binkley, J. S. Derivative Studies in Hartree-Fock and Møller-Plesset Theories. *Int. J. Quantum Chem., Quantum Chem. Symp.* **1979**, *16*, 225.
(18) Raghavachari, K.; Trucks, G. W.; Pople, J. A.; Head-Gordon, M. A fifth-order perturbation comparison of electron correlation theories. *Chem. Phys. Lett.* **1989**, *157*, 479−483.
(19) Feynman, R. P.; Hibbs, A. R. *Quantum Mechanics and Path Integrals*; McGraw-Hill Book Company: New York, 1965.
(20) Meyer, H.-D.; Manthe, U.; Cederbaum, L. S. The multi-configurational time-dependent Hartree approach. *Chem. Phys. Lett.* **1990**, *165*, 73−78.
(21) Nielsen, M. A.; Chuang, I. L. *Quantum computation and quantum information*; Cambridge University Press: Cambridge, 2000.
(22) Feynman, R. P.; Hey, J.; Allen, R. W. *Feynman Lectures on Computation*; Addison-Wesley Longman Publishing Co., Inc., 1998.
(23) Habershon, S.; Manolopoulos, D. E.; Markland, T. E.; Miller, T. F. Ring polymer molecular dynamics: Quantum effects in chemical dynamics from classical trajectories in an extended phase space. *Annu. Rev. Phys. Chem.* **2013**, *64*, 387−413.
(24) DeGregorio, N.; Iyengar, S. S. Adaptive Dimensional Decoupling for Compression of Quantum Nuclear Wave Functions and Efficient Potential Energy Surface Representations through Tensor Network Decomposition. *J. Chem. Theory Comput.* **2019**, *15*, 2780−2796.
(25) DeGregorio, N.; Iyengar, S. S. Efficient and Adaptive Methods for Computing Accurate Potential Surfaces for Quantum Nuclear Effects: Applications to Hydrogen- Transfer Reactions. *J. Chem. Theory Comput.* **2018**, *14*, 30−47.
(26) Ayala, P.; Scuseria, G. Linear scaling second-order Moller−Plesset theory in the atomic orbital basis for large molecular systems. *J. Chem. Phys.* **1999**, *110*, 3660−3671.
(27) Schutz, M.; Werner, H. Low-order scaling local electron correlation methods. IV. Linear scaling local coupled-cluster (LCCSD). *J. Chem. Phys.* **2001**, *114*, 661−681.
(28) Distasio, R. A., Jr.; Steele, R. P.; Rhee, Y. M.; Shao, Y.; Head-Gordon, M. An improved algorithm for analytical gradient evaluation in resolution-of-the-identity second-order Møller-Plesset perturbation theory: Application to alanine tetrapeptide conformational analysis. *J. Comput. Chem.* **2007**, *28*, 839−856.
(29) Pavošević, F.; Pinski, P.; Riplinger, C.; Neese, F.; Valeev, E. F. SparseMaps—A systematic infrastructure for reduced-scaling electronic structure methods. IV. Linear-scaling second-order explicitly correlated energy with pair natural orbitals. *J. Chem. Phys.* **2016**, *144*, 144109.
(30) Sode, O.; Hirata, S. Second-order many-body perturbation study of solid hydrogen fluoride under pressure. *Phys. Chem. Chem. Phys.* **2012**, *14*, 7765.
(31) Iyengar, S. S.; Kouri, D. J.; Hoffman, D. K. Particular and Homogeneous Solutions of Time-Independent Wavepacket Schrodinger Equations: Calculations Using a Subset of Eigenstates of Undamped or Damped Hamiltonians. *Theor. Chem. Acc.* **2000**, *104*, 471−483.
(32) Skone, J. H.; Pak, M. V.; Hammes-Schiffer, S. Nuclear-Electronic Orbital Nonorthogonal Configuration Interaction Approach. *J. Chem. Phys.* **2005**, *123*, 134108.
(33) Iyengar, S. S.; Jakowski, J. Quantum Wavepacket Ab Initio Molecular Dynamics: An Approach to Study Quantum Dynamics in Large Systems. *J. Chem. Phys.* **2005**, *122*, 114105.
(34) Binder, R.; Burghardt, I. First-principles description of intra-chain exciton migration in an oligo(para-phenylene vinylene) chain. II. ML-MCTDH simulations of exciton dynamics at a torsional defect. *J. Chem. Phys.* **2020**, *152*, 204120.
(35) Preskill, J. Quantum Computing in the NISQ era and beyond. *Quantum* **2018**, *2*, 79.
(36) Chia, N.-H.; Chung, K.-M.; Lai, C.-Y. On the Need for Large Quantum Depth. *Proceedings of the 52nd Annual ACM SIGACT Symposium on Theory of Computing. STOC 2020; New York, NY, USA*; Association for Computing Machinery: New York, NY, USA, 2020; pp 902−915.
(37) Porras, D.; Cirac, J. I. Effective Quantum Spin Systems with Trapped Ions. *Phys. Rev. Lett.* **2004**, *92*, 207901.
(38) Richerme, P.; Gong, Z.-X.; Lee, A.; Senko, C.; Smith, J.; Foss-Feig, M.; Michalakis, S.; Gorshkov, A. V.; Monroe, C. Non-local propagation of correlations in quantum systems with long-range interactions. *Nature* **2014**, *511*, 198−201.
(39) Cirac, J. I.; Zoller, P. Quantum Computations with Cold Trapped Ions. *Phys. Rev. Lett.* **1995**, *74*, 4091−4094.
(40) Richerme, P. Two-dimensional ion crystals in radio-frequency traps for quantum simulation. *Phys. Rev. A* **2016**, *94*, 032320.
(41) Barends, R.; Kelly, J.; Megrant, A.; Veitia, A.; Sank, D.; Jeffrey, E.; White, T. C.; Mutus, J.; Fowler, A. G.; Campbell, B.; et al. Superconducting quantum circuits at the surface code threshold for fault tolerance. *Nature* **2014**, *508*, 500−503.
(42) Barends, R.; Lamata, L.; Kelly, J.; García-Álvarez, L.; Fowler, A.; Megrant, A.; Jeffrey, E.; White, T.; Sank, D.; Mutus, J.; et al. Digital quantum simulation of fermionic models with a superconducting circuit. *Nat. Commun.* **2015**, *6*, 7654.
(43) Lanyon, B. P.; Whitfield, J. D.; Gillett, G. G.; Goggin, M. E.; Almeida, M. P.; Kassal, I.; Biamonte, J. D.; Mohseni, M.; Powell, B. J.; Barbieri, M.; et al. Towards quantum chemistry on a quantum computer. *Nat. Chem.* **2010**, *2*, 106−111.
(44) Aspuru-Guzik, A.; Walther, P. Photonic quantum simulators. *Nat. Phys.* **2012**, *8*, 285−291.

https://doi.org/10.1021/acs.jpca.3c04261
J. Phys. Chem. A 2023, 127, 9334−9345

(45) Knill, E.; Laflamme, R.; Milburn, G. J. A scheme for efficient quantum computation with linear optics. *Nature* **2001**, *409*, 46−52.
(46) Pellizzari, T.; Gardiner, S. A.; Cirac, J. I.; Zoller, P. Decoherence, continuous observation, and quantum computing: A cavity QED model. *Phys. Rev. Lett.* **1995**, *75*, 3788−3791.
(47) Loss, D.; DiVincenzo, D. P. Quantum computation with quantum dots. *Phys. Rev. A* **1998**, *57*, 120−126.
(48) Imamoglu, A.; Awschalom, D. D.; Burkard, G.; DiVincenzo, D. P.; Loss, D.; Sherwin, M.; Small, A. Quantum information processing using quantum dot spins and cavity QED. *Phys. Rev. Lett.* **1999**, *83*, 4204−4207.
(49) Calarco, T.; Datta, A.; Fedichev, P.; Pazy, E.; Zoller, P. Spin-based all-optical quantum computation with quantum dots: Understanding and suppressing decoherence. *Phys. Rev. A* **2003**, *68*, 012310.
(50) Saffman, M.; Walker, T. G.; Mølmer, K. Quantum information with Rydberg atoms. *Rev. Mod. Phys.* **2010**, *82*, 2313−2363.
(51) Saffman, M. Quantum computing with atomic qubits and Rydberg interactions: progress and challenges. *J. Phys. B: At., Mol. Opt. Phys.* **2016**, *49*, 202001.
(52) Bernien, H.; Schwartz, S.; Keesling, A.; Levine, H.; Omran, A.; Pichler, H.; Choi, S.; Zibrov, A. S.; Endres, M.; Greiner, M.; et al. Probing many-body dynamics on a 51-atom quantum simulator. *Nature* **2017**, *551*, 579−584.
(53) Jordan, P.; Wigner, E. Über das Paulische Äquivalenzverbot. *Z. Phys.* **1928**, *47*, 631−651.
(54) Ortiz, G.; Gubernatis, J. E.; Knill, E.; Laflamme, R. Quantum algorithms for fermionic simulations. *Phys. Rev. A* **2001**, *64*, 022319.
(55) Bravyi, S. B.; Kitaev, A. Y. Fermionic Quantum Computation. *Ann. Phys.* **2002**, *298*, 210−226.
(56) Aspuru-Guzik, A.; Dutoi, A. D.; Love, P. J.; Head-Gordon, M. Simulated quantum computation of molecular energies. *Science* **2005**, *309*, 1704−1707.
(57) Kirby, W. M.; Love, P. J. Variational Quantum Eigensolvers for Sparse Hamiltonians. *Phys. Rev. Lett.* **2021**, *127*, 110503.
(58) Cervera-Lierta, A.; Kottmann, J. S.; Aspuru-Guzik, A. Meta-Variational Quantum Eigensolver: Learning Energy Profiles of Parameterized Hamiltonians for Quantum Simulation. *PRX Quantum* **2021**, *2*, 020329.
(59) O'Malley, P. J. J.; Babbush, R.; Kivlichan, I. D.; Romero, J.; McClean, J. R.; Barends, R.; Kelly, J.; Roushan, P.; Tranter, A.; Ding, N.; et al. Scalable Quantum Simulation of Molecular Energies. *Phys. Rev. X* **2016**, *6*, 031007.
(60) Smart, S. E.; Mazziotti, D. A. Quantum Solver of Contracted Eigenvalue Equations for Scalable Molecular Simulations on Quantum Computing Devices. *Phys. Rev. Lett.* **2021**, *126*, 070504.
(61) Kandala, A.; Mezzacapo, A.; Temme, K.; Takita, M.; Brink, M.; Chow, J. M.; Gambetta, J. M. Hardware-efficient variational quantum eigensolver for small molecules and quantum magnets. *Nature* **2017**, *549*, 242−246.
(62) Xia, R.; Kais, S. Quantum machine learning for electronic structure calculations. *Nat. Commun.* **2018**, *9*, 4195.
(63) Gorman, D. J.; Hemmerling, B.; Megidish, E.; Moeller, S. A.; Schindler, P.; Sarovar, M.; Haeffner, H. Engineering vibrationally assisted energy transfer in a trapped-ion quantum simulator. *Phys. Rev. X* **2018**, *8*, 011038.
(64) Nam, Y.; Chen, J.-S.; Pisenti, N. C.; Wright, K.; Delaney, C.; Maslov, D.; Brown, K. R.; Allen, S.; Amini, J. M.; Apisdorf, J.; et al. Ground-state energy estimation of the water molecule on a trapped-ion quantum computer. *Npj Quantum Inf.* **2020**, *6*, 33.
(65) Wang, B.-X.; Tao, M.-J.; Ai, Q.; Xin, T.; Lambert, N.; Ruan, D.; Cheng, Y.-C.; Nori, F.; Deng, F.-G.; Long, G.-L. Efficient quantum simulation of photosynthetic light harvesting. *Npj Quantum Inf.* **2018**, *4*, 52.
(66) Chin, A. W.; Mangaud, E.; Atabek, O.; Desouter-Lecomte, M. Coherent quantum dynamics launched by incoherent relaxation in a quantum circuit simulator of a light-harvesting complex. *Phys. Rev. A* **2018**, *97*, 063823.
(67) Potočnik, A.; Bargerbos, A.; Schröder, F. A. Y. N.; Khan, S. A.; Collodo, M. C.; Gasparinetti, S.; Salathé, Y.; Creatore, C.; Eichler, C.; Türeci, H. E.; et al. Studying light-harvesting models with superconducting circuits. *Nat. Commun.* **2018**, *9*, 904.
(68) Peruzzo, A.; McClean, J.; Shadbolt, P.; Yung, M.-H.; Zhou, X.-Q.; Love, P. J.; Aspuru-Guzik, A.; O'brien, J. L. A variational eigenvalue solver on a photonic quantum processor. *Nat. Commun.* **2014**, *5*, 4213.
(69) Grimsley, H. R.; Economou, S. E.; Barnes, E.; Mayhall, N. J. An adaptive variational algorithm for exact molecular simulations on a quantum computer. *Nat. Commun.* **2019**, *10*, 3007.
(70) Arute, F.; Arya, K.; Babbush, R.; Bacon, D.; Bardin, J. C.; Barends, R.; Boixo, S.; Broughton, M.; Buckley, B. B.; Buell, D. A.; et al. Hartree-Fock on a superconducting qubit quantum computer. *Science* **2020**, *369*, 1084−1089.
(71) Parrish, R. M.; Hohenstein, E. G.; McMahon, P. L.; Martinez, T. J. Quantum Computation of Electronic Transitions Using a Variational Quantum Eigensolver. *Phys. Rev. Lett.* **2019**, *122*, 230401.
(72) Tkachenko, N. V.; Sud, J.; Zhang, Y.; Tretiak, S.; Anisimov, P. M.; Arrasmith, A. T.; Coles, P. J.; Cincio, L.; Dub, P. A. Correlation-Informed Permutation of Qubits for Reducing Ansatz Depth in the Variational Quantum Eigensolver. *PRX Quantum* **2021**, *2*, 020337.
(73) Huggins, W. J.; McClean, J. R.; Rubin, N. C.; Jiang, Z.; Wiebe, N.; Whaley, K. B.; Babbush, R. Efficient and noise resilient measurements for quantum chemistry on near-term quantum computers. *Npj Quantum Inf.* **2021**, *7*, 23.
(74) McClean, J. R.; Rubin, N. C.; Sung, K. J.; Kivlichan, I. D.; Bonet-Monroig, X.; Cao, Y.; Dai, C.; Fried, E. S.; Gidney, C.; Gimby, B.; et al. OpenFermion: the electronic structure package for quantum computers. *Quantum Sci. Technol.* **2020**, *5*, 034014.
(75) Motta, M.; Gujarati, T. P.; Rice, J. E.; Kumar, A.; Masteran, C.; Latone, J. A.; Lee, E.; Valeev, E. F.; Takeshita, T. Y. Quantum simulation of electronic structure with a transcorrelated Hamiltonian: improved accuracy with a smaller footprint on the quantum computer. *Phys. Chem. Chem. Phys.* **2020**, *22*, 24270−24281.
(76) Lang, R. A.; Ryabinkin, I. G.; Izmaylov, A. F. Unitary Transformation of the Electronic Hamiltonian with an Exact Quadratic Truncation of the Baker-Campbell-Hausdorff Expansion. *J. Chem. Theory Comput.* **2021**, *17*, 66−78.
(77) Ryabinkin, I. G.; Yen, T.-C.; Genin, S. N.; Izmaylov, A. F. Qubit Coupled Cluster Method: A Systematic Approach to Quantum Chemistry on a Quantum Computer. *J. Chem. Theory Comput.* **2018**, *14*, 6317−6326.
(78) Izmaylov, A. F.; Yen, T.-C.; Lang, R. A.; Verteletskyi, V. Unitary Partitioning Approach to the Measurement Problem in the Variational Quantum Eigensolver Method. *J. Chem. Theory Comput.* **2020**, *16*, 190−195.
(79) Zhang, J. H.; Iyengar, S. S. Graph-$|Q\rangle\langle C|$: A Graph-based Quantum-classical algorithm for efficient electronic structure on hybrid quantum/classical hardware systems: Improved quantum circuit depth performance. *J. Chem. Theory Comput.* **2022**, *18*, 2885−2899.
(80) Iyengar, S. S.; Saha, D.; Dwivedi, A.; Lopez-Ruiz, M. A.; Kumar, A.; Zhang, J. H.; Ricard, T. C.; Richerme, P.; Sabry, A. Quantum Algorithms for the Study of Electronic Structure and Molecular Dynamics: Novel Computational Protocols. *Comprehensive Computational Chemistry*; Elsevier, 2023.
(81) Kassal, I.; Jordan, S. P.; Love, P. J.; Mohseni, M.; Aspuru-Guzik, A. Polynomial-time quantum algorithm for the simulation of chemical dynamics. *Proc. Natl. Acad. Sci. U.S.A.* **2008**, *105*, 18681−18686.
(82) MacDonell, R. J.; Dickerson, C. E.; Birch, C. J. T.; Kumar, A.; Edmunds, C. L.; Biercuk, M. J.; Hempel, C.; Kassal, I. Analog quantum simulation of chemical dynamics. *Chem. Sci.* **2021**, *12*, 9794−9805.
(83) Ollitrault, P. J.; Baiardi, A.; Reiher, M.; Tavernelli, I. Hardware efficient quantum algorithms for vibrational structure calculations. *Chem. Sci.* **2020**, *11*, 6842−6855.
(84) Sawaya, N. P.; Menke, T.; Kyaw, T. H.; Johri, S.; Aspuru-Guzik, A.; Guerreschi, G. G. Resource-efficient digital quantum simulation of d-level systems for photonic, vibrational, and spin-s Hamiltonians. *Npj Quantum Inf.* **2020**, *6*, 49.
(85) Teplukhin, A.; Kendrick, B. K.; Babikov, D. Solving complex eigenvalue problems on a quantum annealer with applications to

https://doi.org/10.1021/acs.jpca.3c04261
J. Phys. Chem. A 2023, 127, 9334−9345

quantum scattering resonances. *Phys. Chem. Chem. Phys.* **2020**, *22*, 26136−26144.
(86) Jahangiri, S.; Arrazola, J. M.; Quesada, N.; Delgado, A. Quantum algorithm for simulating molecular vibrational excitations. *Phys. Chem. Chem. Phys.* **2020**, *22*, 25528−25537.
(87) Wang, C. S.; Curtis, J. C.; Lester, B. J.; Zhang, Y.; Gao, Y. Y.; Freeze, J.; Batista, V. S.; Vaccaro, P. H.; Chuang, I. L.; Frunzio, L.; et al. Efficient Multiphoton Sampling of Molecular Vibronic Spectra on a Superconducting Bosonic Processor. *Phys. Rev. X* **2020**, *10*, 021060.
(88) Saha, D.; Iyengar, S. S.; Richerme, P.; Smith, J. M.; Sabry, A. Mapping Quantum Chemical Dynamics Problems to Spin-Lattice Simulators. *J. Chem. Theory Comput.* **2021**, *17*, 6713−6732.
(89) Richerme, P.; Revelle, M. C.; Yale, C. G.; Lobser, D.; Burch, A. D.; Clark, S. M.; Saha, D.; Lopez-Ruiz, M. A.; Dwivedi, A.; Smith, J. M.; et al. Quantum Computation of Hydrogen Bond Dynamics and Vibrational Spectra. *J. Phys. Chem. Lett.* **2023**, *14*, 7256−7263.
(90) Preskill, J. Quantum Computing and the Entanglement Frontier. *arXiv* **2012**, arXiv:1203.5813. [quant-ph]
(91) Aleksandrowicz, G.; Alexander, T.; Barkoutsos, P.; Bello, L.; Ben-Haim, Y.; Bucher, D.; Cabrera-Hernández, F. J.; Carballo-Franquis, J.; Chen, A.; Chen, C.-F.; et al. *Qiskit: An Open-source Framework for Quantum Computing*, 2019.
(92) Shen, Y.; Zhang, X.; Zhang, S.; Zhang, J.-N.; Yung, M.-H.; Kim, K. Quantum implementation of the unitary coupled cluster for simulating molecular electronic structure. *Phys. Rev. A* **2017**, *95*, 020501.
(93) Grimsley, H. R.; Claudino, D.; Economou, S. E.; Barnes, E.; Mayhall, N. J. Is the Trotterized UCCSD Ansatz Chemically Well-Defined? *J. Chem. Theory Comput.* **2020**, *16*, 1−6.
(94) Bravyi, S.; Gambetta, J. M.; Mezzacapo, A.; Temme, K. Tapering off qubits to simulate fermionic Hamiltonians. *arXiv* **2017**, arXiv:1701.08213. preprint
(95) Kraft, D. *A software package for sequential quadratic programming*; Wiss. Berichtswesen d. DFVLR Brunswick: Germany, 1988.
(96) Drury, B.; Love, P. Constructive quantum Shannon decomposition from Cartan involutions. *J. Phys. A: Math. Theor.* **2008**, *41*, 395305.
(97) Shende, V.; Bullock, S.; Markov, I. Synthesis of quantum-logic circuits. *IEEE Trans. Comput.-Aided Des. Integr. Circuits Syst.* **2006**, *25*, 1000−1010.
(98) Sutton, B. D. Computing the complete CS decomposition. *Numer. Algorithms* **2009**, *50*, 33−65.
(99) Kühn, M.; Zanker, S.; Deglmann, P.; Marthaler, M.; Weiß, H. Accuracy and Resource Estimations for Quantum Chemistry on a Near-Term Quantum Computer. *J. Chem. Theory Comput.* **2019**, *15*, 4764−4780.
(100) Kandala, A.; Wei, K. X.; Srinivasan, S.; Magesan, E.; Carnevale, S.; Keefe, G. A.; Klaus, D.; Dial, O.; McKay, D. C. Demonstration of a High-Fidelity cnot Gate for Fixed-Frequency Transmons with Engineered *ZZ* Suppression. *Phys. Rev. Lett.* **2021**, *127*, 130501.
(101) Maseras, F.; Morokuma, K. IMOMM: A new integrated ab initio + molecular mechanics geometry optimization scheme of equilibrium structures and transition states. *J. Comput. Chem.* **1995**, *16*, 1170−1179.
(102) Frisch, M. J.; Trucks, G. W.; Schlegel, H. B.; Scuseria, G. E.; Robb, M. A.; Cheeseman, J. R.; Scalmani, G.; Barone, V.; Petersson, G. A.; Nakatsuji, H.; et al. *Gaussian 16*, Revision B.01; Gaussian Inc: Wallingford CT, 2016.
(103) Parrish, R. M.; Burns, L. A.; Smith, D. G. A.; Simmonett, A. C.; DePrince, A. E., III; Hohenstein, E. G.; Bozkaya, U.; Sokolov, A. Y.; Di Remigio, R.; Richard, R. M.; et al. PSI4 1.1: An Open-Source Electronic Structure Program Emphasizing Automation, Advanced Libraries, and Interoperability. *J. Chem. Theory Comput.* **2017**, *13*, 3185−3197.
(104) Neese, F. The ORCA program system. *Wiley Interdiscip. Rev.: Comput. Mol. Sci.* **2012**, *2*, 73−78.
(105) Giannozzi, P.; Baroni, S.; Bonini, N.; Calandra, M.; Car, R.; Cavazzoni, C.; Ceresoli, D.; Chiarotti, G. L.; Cococcioni, M.; Dabo, I.; et al. QUANTUM ESPRESSO: a modular and open-source software project for quantum simulations of materials. *J. Phys.: Condens.Matter* **2009**, *21*, 395502.
(106) Björklund, A.; Husfeldt, T.; Koivisto, M. Set Partitioning via Inclusion Exclusion. *SIAM J. Comput.* **2009**, *39*, 546−563.
(107) Dey, T. K.; Shah, N. R. On the number of simplicial complexes in Rd. *Comput. Geom.* **1997**, *8*, 267−277.
(108) Adams, C. C.; Franzosa, R. D. *Introduction to topology: pure and applied*; Pearson Prentice Hall, 2008.
(109) Berger, M.; Pansu, P.; Berry, J.-P.; Saint-Raymond, X. Affine spaces. *Problems in Geometry*; Springer, 1984; p 11.
(110) Varandas, A. J.; Murrell, J. N. A many-body expansion of polyatomic potential energy surfaces: application to H_n systems. *Faraday Discuss. Chem. Soc.* **1977**, *62*, 92.
(111) Dahlke, E. E.; Truhlar, D. G. Electrostatically Embedded Many Body Expansion for Large Systems, with Applications to Water Clusters. *J. Chem. Theory Comput.* **2007**, *3*, 46−53.
(112) Dahlke, E. E.; Truhlar, D. G. Electrostatically Embedded Many Body Expansion for Simulations. *J. Chem. Theory Comput.* **2008**, *4*, 1−6.
(113) Jacobson, L. D.; Herbert, J. M. An Efficient, Fragment-Based Electronic Structure Method for Molecular Systems: Self-Consistent Polarization with Perturbative Two-Body Exchange and Dispersion. *J. Chem. Phys.* **2011**, *134*, 094118.
(114) Richard, R. M.; Herbert, J. M. A Generalized Many-Body Expansion and a Unified View of Fragment-Based Methods in Electronic Structure Theory. *J. Chem. Phys.* **2012**, *137*, 064113.
(115) Ricard, T. C.; Iyengar, S. S. Efficient and Accurate Approach To Estimate Hybrid Functional and Large Basis-Set Contributions to Condensed-Phase Systems and Molecule−Surface Interactions. *J. Chem. Theory Comput.* **2020**, *16*, 4790−4812.
(116) Zhang, J. H.; Ricard, T. C.; Haycraft, C.; Iyengar, S. S. Weighted-Graph-Theoretic Methods for Many-Body Corrections within ONIOM: Smooth AIMD and the Role of High-Order Many-Body Terms. *J. Chem. Theory Comput.* **2021**, *17*, 2672−2690.
(117) Li, J.; Iyengar, S. S. Ab initio Molecular Dynamics using Recursive, Spatially Separated, Overlapping Model Subsystems Mixed Within an ONIOM Based Fragmentation Energy Extrapolation Technique. *J. Chem. Theory Comput.* **2015**, *11*, 3978−3991.
(118) Li, J.; Haycraft, C.; Iyengar, S. S. Hybrid Extended Lagrangian, Post-Hartree−Fock Born−Oppenheimer ab Initio Molecular Dynamics Using Fragment-Based Electronic Structure. *J. Chem. Theory Comput.* **2016**, *12*, 2493−2508.
(119) Haycraft, C.; Li, J.; Iyengar, S. S. Efficient, "On-the-fly" Born−Oppenheimer and Car−Parrinello−type Dynamics with coupled cluster accuracy through Fragment Based Electronic Structure. *J. Chem. Theory Comput.* **2017**, *13*, 21887−21901.
(120) Ricard, T. C.; Haycraft, C.; Iyengar, S. S. Adaptive, geometric networks for efficient coarse-grained *ab initio* molecular dynamics with post-Hartree-Fock accuracy. *J. Chem. Theory Comput.* **2018**, *14*, 2852−2866.
(121) Ricard, T. C.; Iyengar, S. S. Efficiently Capturing Weak Interactions in ab Initio Molecular Dynamics with on-the-Fly Basis Set Extrapolation. *J. Chem. Theory Comput.* **2018**, *14*, 5535−5552.
(122) Kumar, A.; Iyengar, S. S. Fragment-based electronic structure for potential energy surfaces using a superposition of fragmentation topologies. *J. Chem. Theory Comput.* **2019**, *15*, 5769−5786.
(123) Ricard, T. C.; Kumar, A.; Iyengar, S. S. Embedded, graph-theoretically defined many-body approximations for wavefunction-in-DFT and DFT-in-DFT: Applications to gas- and condensed-phase ab initio molecular dynamics, and potential surfaces for quantum nuclear effects. *Int. J. Quantum Chem.* **2020**, *120*, No. e26244.
(124) Kumar, A.; DeGregorio, N.; Iyengar, S. S. Graph-Theory-Based Molecular Fragmentation for Efficient and Accurate Potential Surface Calculations in Multiple Dimensions. *J. Chem. Theory Comput.* **2021**, *17*, 6671−6690.
(125) Kumar, A.; DeGregorio, N.; Ricard, T.; Iyengar, S. S. Graph-Theoretic Molecular Fragmentation for Potential Surfaces Leads Naturally to a Tensor Network Form and Allows Accurate and Efficient Quantum Nuclear Dynamics. *J. Chem. Theory Comput.* **2022**, *18*, 7243−7259.

https://doi.org/10.1021/acs.jpca.3c04261
J. Phys. Chem. A 2023, 127, 9334−9345

(126) Zhu, X.; Iyengar, S. S. Graph Theoretic Molecular Fragmentation for Multidimensional Potential Energy Surfaces Yield an Adaptive and General Transfer Machine Learning Protocol. *J. Chem. Theory Comput.* **2022**, *18*, 5125−5144.
(127) Nyden, M.; Petersson, G. Complete basis set correlation energies. I. The asymptotic convergence of pair natural orbital expansions. *J. Chem. Phys.* **1981**, *75*, 1843−1862.
(128) Pople, J.; Head-Gordon, M.; Fox, D.; Raghavachari, K.; Curtiss, L. Gaussian-1 theory: A general procedure for prediction of molecular energies. *J. Chem. Phys.* **1989**, *90*, 5622−5629.
(129) Montgomery, J.; Frisch, M.; Ochterski, J.; Petersson, G. A complete basis set model chemistry. VI. Use of density functional geometries and frequencies. *J. Chem. Phys.* **1999**, *110*, 2822−2827.
(130) DeYonker, N.; Cundari, T.; Wilson, A. The correlation consistent composite approach (ccCA): An alternative to the Gaussian-n methods. *J. Chem. Phys.* **2006**, *124*, 114104.
(131) Raghavachari, K.; Saha, A. Accurate Composite and Fragment-Based Quantum Chemical Models for Large Molecules. *Chem. Rev.* **2015**, *115*, 5643−5677.
(132) Kerdcharoen, T.; Morokuma, K. ONIOM-XS: An Extension of the ONIOM Method for Molecular Simulation in Condensed Phase. *Chem. Phys. Lett.* **2002**, *355*, 257−262.
(133) Hopkins, B. W.; Tschumper, G. S. A multicentered approach to integrated QM/QM calculations. Applications to multiply hydrogen bonded systems. *J. Comput. Chem.* **2003**, *24*, 1563−1568.
(134) Guo, W.; Wu, A.; Xu, X. XO: An Extended ONIOM Method for Accurate and Efficient Geometry Optimization of Large Molecules. *Chem. Phys. Lett.* **2010**, *498*, 203−208.
(135) Mayhall, N. J.; Raghavachari, K. Molecules-In-Molecules: An Extrapolated Fragment-Based Approach for Accurate Calculations on Large Molecules and Materials. *J. Chem. Theory Comput.* **2011**, *7*, 1336−1343.
(136) Mayhall, N. J.; Raghavachari, K. Many-Overlapping-Body (MOB) Expansion: A Generalized Many Body Expansion for Nondisjoint Monomers in Molecular Fragmentation Calculations of Covalent Molecules. *J. Chem. Theory Comput.* **2012**, *8*, 2669−2675.
(137) Beran, G. J. O. Modeling polymorphic molecular crystals with electronic structure theory. *Chem. Rev.* **2016**, *116*, 5567−5613.
(138) Zhang, D. W.; Zhang, J. Z. H. Molecular Fractionation with Conjugate Caps for Full Quantum Mechanical Calculation of Protein−molecule Interaction Energy. *J. Chem. Phys.* **2003**, *119*, 3599−3605.
(139) Huang, L.; Massa, L.; Karle, J. Kernel energy method: Application to DNA. *Biochem* **2005**, *44*, 16747−16752.
(140) Ganesh, V.; Dongare, R. K.; Balanarayan, P.; Gadre, S. R. Molecular Tailoring Approach for Geometry Optimization of Large Molecules: Energy Evaluation and Parallelization Strategies. *J. Chem. Phys.* **2006**, *125*, 104109.
(141) Le, H.-A.; Tan, H.-J.; Ouyang, J. F.; Bettens, R. P. A. Combined Fragmentation Method: A Simple Method for Fragmentation of Large Molecules. *J. Chem. Theory Comput.* **2012**, *8*, 469−478.
(142) Li, S.; Li, W.; Ma, J. Generalized Energy-Based Fragmentation Approach and Its Applications to Macromolecules and Molecular Aggregates. *Acc. Chem. Res.* **2014**, *47*, 2712−2720.
(143) Gordon, M.; Mullin, J.; Pruitt, S.; Roskop, L.; Slipchenko, L.; Boatz, J. Accurate Methods for Large Molecular Systems. *J. Phys. Chem. B* **2009**, *113*, 9646−9663.
(144) Collins, M. A.; Bettens, R. P. A. Energy-Based Molecular Fragmentation Methods. *Chem. Rev.* **2015**, *115*, 5607−5642.
(145) Collins, M. A. Systematic Fragmentation of Large Molecules by Annihilation. *Phys. Chem. Chem. Phys.* **2012**, *14*, 7744.
(146) Willow, S. Y.; Salim, M. A.; Kim, K. S.; Hirata, S. Ab initio molecular dynamics of liquid water using embedded-fragment second-order many-body perturbation theory towards its accurate property prediction. *Sci. Rep.* **2015**, *5*, 14358.
(147) Han, J.; Mazack, M. J. M.; Zhang, P.; Truhlar, D. G.; Gao, J. Quantum Mechanical Force Field for Water with Explicit Electronic Polarization. *J. Chem. Phys.* **2013**, *139*, 054503.
(148) Liu, J.; Qi, L.-W.; Zhang, J. Z. H.; He, X. Fragment Quantum Mechanical Method for Large-Sized Ion−Water Clusters. *J. Chem. Theory Comput.* **2017**, *13*, 2021−2034.
(149) Herbert, J. M. Fantasy versus reality in fragment-based quantum chemistry. *J. Chem. Phys.* **2019**, *151*, 170901.
(150) Murrell, J.; Carter, S.; Farantos, S.; Huxley, P.; Varandas, A. *Molecular Potential Energy Functions*; Wiley: New York, 1984.
(151) Varandas, A.; Pais, A. A realistic double many-body expansion (DMBE) potential energy surface for ground-state O_3 from a multiproperty fit to ab initio calculations, and to experimental spectroscopic, inelastic scattering, and kinetic isotope thermal rate data. *Mol. Phys.* **1988**, *65*, 843−860.
(152) Xantheas, S. S. *Ab Initio* Studies of Cyclic Water Clusters $(H_2O)_n$, N = 1−6. II. Analysis of Many-body Interactions. *J. Chem. Phys.* **1994**, *100*, 7523−7534.
(153) Xantheas, S. S. *Ab Initio* Studies of Cyclic Water Clusters $(H_2O)_n$, N = 1−6. III. Comparison of Density Functional with MP2 Results. *J. Chem. Phys.* **1995**, *102*, 4505−4517.
(154) Hirata, S. Fast Electron-Correlation Methods for Molecular Crystals: an Application to the α, $\beta(1)$, and $\beta(2)$ Modifications of Solid Formic Acid. *J. Chem. Phys.* **2008**, *129*, 204104.
(155) Yu, Q.; Bowman, J. M. Communication: VSCF/VCI vibrational spectroscopy of $H_7O_3^+$ and $H_9O_4^+$ using high-level, many-body potential energy surface and dipole moment surfaces. *J. Chem. Phys.* **2017**, *146*, 121102.
(156) Yang, J.; Hu, W.; Usvyat, D.; Matthews, D.; Schütz, M.; Chan, G. K.-L. Ab initio determination of the crystalline benzene lattice energy to sub-kilojoule/mole accuracy. *Science* **2014**, *345*, 640−643.
(157) Georges, A.; Kotliar, G.; Krauth, W.; Rozenberg, M. J. Dynamical mean-field theory of strongly correlated fermion systems and the limit of infinite dimensions. *Rev. Mod. Phys.* **1996**, *68*, 13−125.
(158) Kotliar, G.; Savrasov, S. Y.; Haule, K.; Oudovenko, V. S.; Parcollet, O.; Marianetti, C. A. Electronic structure calculations with dynamical mean-field theory. *Rev. Mod. Phys.* **2006**, *78*, 865−951.
(159) Polkosnik, W.; Massa, L. Kohn-Sham Density Matrix and the Kernel Energy Method. *Acta Phys.-Chim. Sin.* **2018**, *34*, 656.
(160) Sun, Q.; Chan, G. K.-L. Quantum Embedding Theories. *Acc. Chem. Res.* **2016**, *49*, 2705−2712.
(161) Faulstich, F. M.; Kim, R.; Cui, Z.-H.; Wen, Z.; Kin-Lic Chan, G.; Lin, L. Pure State v-Representability of Density Matrix Embedding Theory. *J. Chem. Theory Comput.* **2022**, *18*, 851−864.
(162) Nguyen Lan, T.; Kananenka, A. A.; Zgid, D. Rigorous Ab Initio Quantum Embedding for Quantum Chemistry Using Green's Function Theory: Screened Interaction, Nonlocal Self-Energy Relaxation, Orbital Basis, and Chemical Accuracy. *J. Chem. Theory Comput.* **2016**, *12*, 4856−4870.
(163) Ma, H.; Govoni, M.; Galli, G. Quantum simulations of materials on near-term quantum computers. *npj Comput. Mater.* **2020**, *6*, 85.
(164) Baciou, L.; Michel, H. Interruption of the water chain in the reaction center from Rhodobacter sphaeroides reduces the rates of the proton uptake and of the second electron transfer to QB. *Biochemistry* **1995**, *34*, 7967−7972.
(165) Guo, H.; Barnard, A. S. Proton transfer in the hydrogen-bonded chains of lepidocrocite: a computational study. *Phys. Chem. Chem. Phys.* **2011**, *13*, 17864.
(166) Domene, C.; Sansom, M. S. Potassium channel, ions, and water: simulation studies based on the high resolution X-ray structure of KcsA. *Biophys. J.* **2003**, *85*, 2787−2800.
(167) Mann, D. J.; Halls, M. D. Water Alignment and Proton Conduction inside Carbon Nanotubes. *Phys. Rev. Lett.* **2003**, *90*, 195503.
(168) Song, W.; Joshi, H.; Chowdhury, R.; Najem, J. S.; Shen, Y.-X.; Lang, C.; Henderson, C. B.; Tu, Y.-M.; Farell, M.; Pitz, M. E.; et al. Artificial water channels enable fast and selective water permeation through water-wire networks. *Nat. Nanotechnol.* **2020**, *15*, 73−79.
(169) Hummer, G.; Rasaiah, J. C.; Noworyta, J. P. Water conduction through the hydrophobic channel of a carbon nanotube. *Nature* **2001**, *414*, 188−190.

https://doi.org/10.1021/acs.jpca.3c04261
J. Phys. Chem. A 2023, 127, 9334−9345

(170) Ye, Y.-S.; Rick, J.; Hwang, B.-J. Water soluble polymers as proton exchange membranes for fuel cells. *Polymers* **2012**, *4*, 913−963.
(171) Tuckerman, M. E.; Ungar, P. J.; Vonrosenvinge, T.; Klein, M. L. Ab Initio Molecular Dynamics Simulations. *J. Phys. Chem.* **1996**, *100*, 12878−12887.
(172) Tuckerman, M.; Laasonen, K.; Sprik, M.; Parrinello, M. Ab Initio Molecular Dynamics Simulation of the Solvation and Transport of H3O+ and OH- Ions in Water. *J. Phys. Chem.* **1995**, *99*, 5749−5752.
(173) Schmitt, U. W.; Voth, G. A. The computer simulation of proton transport in water. *J. Chem. Phys.* **1999**, *111*, 9361−9381.
(174) Schmitt, U. W.; Voth, G. A. Multistate empirical valence bond model for proton transport in water. *J. Phys. Chem. B* **1998**, *102*, 5547−5551.
(175) Shin, J.-W.; Hammer, N. I.; Diken, E. G.; Johnson, M. A.; Walters, R. S.; Jaeger, T. D.; Duncan, M. A.; Christie, R. A.; Jordan, K. D. Infrared Signature of Structures Associated with the $H^+(H_2O)_n$ (N = 6 to 27) Clusters. *Science* **2004**, *304*, 1137−1140.
(176) Headrick, J. M.; Diken, E. G.; Walters, R. S.; Hammer, N. I.; Christie, R. A.; Cui, J.; Myshakin, E. M.; Duncan, M. A.; Johnson, M. A.; Jordan, K. Spectral Signatures of Hydrated Proton Vibrations in Water Clusters. *Science* **2005**, *308*, 1765−1769.
(177) Deumens, E.; Diz, A.; Longo, R.; Öhrn, Y. Time-Dependent Theoretical Treatments of the Dynamics of Electrons and Nuclei in Molecular-Systems. *Rev. Mod. Phys.* **1994**, *66*, 917−983.
(178) Riesz, F.; Sz.-Nagy, B. *Functional Analysis*; Dover Publications, Inc.: Mineola, NY, 1990.

https://doi.org/10.1021/acs.jpca.3c04261
J. Phys. Chem. A 2023, 127, 9334−9345